

- Chem. Int. Ed. Engl.* **30**, 1417 (1991); K. Araki, H. Shimizu, S. Shinkai, *Chem. Lett.*, 205 (1993).
28. S. Dao-pin, U. Sauer, H. Nicholson, B. W. Matthews, *Biochemistry* **30**, 7142 (1991); Z. S. Hendsch and B. Tidor, *Protein Sci.* **3**, 211 (1994); C. D. Waldburger, J. F. Schildbach, R. T. Sauer, *Struct. Biol.* **2**, 122 (1995).
  29. D. A. Stauffer, R. E. Barrans Jr., D. A. Dougherty, *Angew. Chem. Int. Ed. Engl.* **29**, 915 (1990); A. McCurdy, L. Jimenez, D. A. Stauffer, D. A. Dougherty, *J. Am. Chem. Soc.* **114**, 10314 (1992).
  30. M. F. Perutz, G. Fermi, D. J. Abraham, C. Poyart, E. Bursaux, *J. Am. Chem. Soc.* **108**, 1064 (1986); M. F. Perutz, *Philos. Trans. R. Soc. London Ser. A* **345**, 105 (1993).
  31. S. K. Burley and G. A. Petsko, *FEBS Lett.* **203**, 139 (1986); *Weakly Polar Interactions in Proteins*, vol. 39 of *Advances in Protein Chemistry* (Academic Press, New York, 1988).
  32. J. B. O. Mitchell *et al.*, *Nature* **366**, 413 (1993); J. B. O. Mitchell, C. L. Nandi, I. K. McDonald, J. M. Thornton, S. L. Price, *J. Mol. Biol.* **239**, 315 (1994).
  33. C. L. Nandi, J. Singh, J. M. Thornton, *Protein Eng.* **6**, 247 (1993); E. M. Duffy, P. J. Kowalczyk, W. L. Jorgensen, *J. Am. Chem. Soc.* **115**, 9271 (1993); M. M. Flocco and S. L. Mowbray, *J. Mol. Biol.* **235**, 709 (1994).
  34. D. A. Dougherty and D. A. Stauffer, *Science* **250**, 1558 (1990).
  35. Y. Satow, G. H. Cohen, E. A. Padlan, D. R. Davies, *J. Mol. Biol.* **190**, 593 (1986); J. Novotny, R. E. Brucoleri, F. A. Saul, *Biochemistry* **28**, 4735 (1989).
  36. J. L. Sussman *et al.*, *Science* **253**, 872 (1991). For a review, see J. L. Sussman and I. Silman, *Curr. Opin. Struct. Biol.* **2**, 721 (1992).
  37. The gas-phase interaction of  $N(CH_3)_4^+$  with water is comparable to its interaction with benzene (7), which establishes that an OH can bind a cation through electrostatic interactions.
  38. For lead references on the nAChR, see (39) as well as A. Karlin, *Curr. Opin. Neurobiol.* **3**, 299 (1993); S. N. Abramson, W. Fenical, P. Taylor, *Drug Dev. Res.* **24**, 297 (1991); J. B. Cohen, S. D. Sharp, W. S. Liu, *J. Biol. Chem.* **266**, 23354 (1991); T. L. Lentz, *Biochemistry* **34**, 1316 (1995); Y. Fraenkel, J. M. Gershoni, G. Navon, *FEBS Lett.* **291**, 225 (1991); M. W. Nowak *et al.*, *Science* **268**, 439 (1995).
  39. J.-L. Galzi, F. Revah, A. Bessis, J.-P. Changeux, *Annu. Rev. Pharmacol.* **31**, 37 (1991); J.-L. Galzi and J.-P. Changeux, *Curr. Opin. Struct. Biol.* **4**, 554 (1994).
  40. N. Unwin, *J. Mol. Biol.* **229**, 1101 (1993).
  41. Evidence also exists for more classical (ion-pair) electrostatic interactions contributing to the binding in the nAChR [C. Czajkowski, C. Kaufmann, A. Karlin, *Proc. Natl. Acad. Sci. U.S.A.* **90**, 6285 (1993)].
  42. D. Donnelly and J. B. C. Findlay, *Curr. Opin. Struct. Biol.* **4**, 582 (1994).
  43. S. Trumpp-Kallmeyer, J. Hoflack, A. Bruinvels, M. Hibert, *J. Med. Chem.* **35**, 3448 (1992).
  44. M. F. Hibert, S. Trumpp-Kallmeyer, A. Bruinvels, J. Hoflack, *Mol. Pharmacol.* **40**, 8 (1991).
  45. J. Wess, R. Maggio, J. R. Palmer, Z. Vogel, *J. Biol. Chem.* **267**, 19313 (1992); G. Nordvall and U. Hacksell, *J. Med. Chem.* **36**, 967 (1993).
  46. H. Moereels and J. E. Leysen, *Receptors Channels* **1**, 89 (1993).
  47. For reviews, see C. Miller, *Science* **252**, 1092 (1991); B. A. Wible and A. M. Brown, *Drug Dev. Res.* **33**, 225 (1994).
  48. In a few of the  $K^+$ -selective channels, Gly-Tyr-Gly is replaced by Gly-Phe-Gly.
  49. L. Heginbotham and R. MacKinnon, *Neuron* **8**, 483 (1992).
  50. Some support for this proposal comes from computational models of the channel [S. R. Durell and H. R. Guy, *Biophys. J.* **62**, 238 (1992); S. Bogusz, A. Boxer, D. D. Busath, *Protein Eng.* **5**, 285 (1992)].
  51. MacKinnon and co-workers recently showed that a mutant channel with Gly-Tyr-Gly replaced by Gly-Val-Gly can display some  $K^+$  selectivity [L. Heginbotham, Z. Lu, T. Abramson, R. MacKinnon, *Biophys. J.* **66**, 1061 (1994)], but not the very high selectivity that defines this class of  $K^+$  channels.
  52. R. MacKinnon and G. Yellen, *Science* **250**, 276 (1990); G. Yellen, M. E. Jurman, T. Abramson, R. MacKinnon, *ibid.* **251**, 939 (1991); M. P. Kavanaugh *et al.*, *Neuron* **8**, 493 (1992).
  53. J. Satin *et al.*, *Science* **256**, 1202 (1992); P. H. Backx, D. T. Yue, J. H. Lawrence, E. Marban, G. F. Tomaselli, *ibid.* **257**, 248 (1992); L.-Q. Chen, M. Chahine, R. G. Kallen, R. L. Barchi, R. Horn, *FEBS Lett.* **309**, 253 (1992).
  54. G. L. Cantoni, *Annu. Rev. Biochem.* **49**, 435 (1975); G. A. Maw, in *The Chemistry of the Sulphonium Group*, C. J. M. Stirling and S. Patai, Eds. (Wiley, New York, 1981), chap. 17; E. Q. Lederer, *Rev. Chem. Soc.* **23**, 453 (1969); C. Walsh, *Enzyme Reaction Mechanisms* (Freeman, New York, 1979), pp. 851-863.
  55. X. Cheng, S. Kumar, J. Posfai, J. W. Pflugrath, R. J. Roberts, *Cell* **74**, 299 (1993).
  56. Electrostatic maps similar to those of Fig. 2 indicate that, in a trialkylsulfonium system, the site of greatest positive electrostatic potential is at the sulfur, consistent with the alignment of Fig. 5 (A. McCurdy and D. A. Dougherty, unpublished results).
  57. R. M. Kagan and S. Clarke, *Arch. Biochem. Biophys.* **310**, 417 (1994).
  58. W. S. Johnson, S. D. Lindell, J. Steele, *J. Am. Chem. Soc.* **109**, 5882 (1987).
  59. K. Poralla *et al.*, *Trends Biochem. Sci.* **19**, 157 (1994); Z. Shi, C. J. Buntel, J. H. Griffin, *Proc. Natl. Acad. Sci. U.S.A.* **91**, 7370 (1994); C. J. Buntel and J. H. Griffin, in *Isopentenoids and Other Natural Products* (American Chemical Society, Washington, DC, 1994), pp. 44-54; D. Ochs, C. Kaletta, K. D. Entian, A. Becksickinger, K. Poralla, *J. Bacteriol.* **174**, 298 (1992); C. A. Roessner *et al.*, *Gene* **127**, 149 (1993).
  60. R. Loewenthal, J. Sancho, A. R. Fersht, *J. Mol. Biol.* **224**, 759 (1992).
  61. G. Waksman, *Cell. Mol. Biol.* **40**, 611 (1994).
  62. J. L. Jorgensen, U. Esser, B. Fazekas de St. Groth, P. A. Reay, M. M. Davis, *Nature* **355**, 224 (1992).
  63. A. R. Ortiz, T. Pisabarro, J. Gallego, F. Gago, *Biochemistry* **31**, 2887 (1992).
  64. L. Brocchieri and S. Karlin, *Proc. Natl. Acad. Sci. U.S.A.* **91**, 9297 (1994); S. Karlin, M. Zuker, L. Brocchieri, *J. Mol. Biol.* **239**, 227 (1994).
  65. S. W. Cowan and J. P. Rosenbusch, *Science* **264**, 914 (1994).
  66. Aromatic residues appear with abnormally high frequencies at many types of biological binding sites, even those not necessarily targeted to cations. These include the binding sites of antibodies [I. S. Mian, A. R. Bradwell, A. J. Olson, *J. Mol. Biol.* **217**, 133 (1991)] and the transmembrane regions of multidrug resistance proteins [A. B. Pawagi, J. Wang, M. Silverman, R. A. F. Reithmeier, C. M. Deber, *ibid.* **235**, 554 (1994)].
  67. Contribution No. 9016 from the Arnold and Mabel Beckman Laboratories of Chemical Synthesis. Supported by NIH (GM43936), the Office of Naval Research (N00014-91-J-1344), and Zeneca Pharmaceuticals. D.A.D. thanks many outstanding students and postdoctoral colleagues for their contributions to this work.

## Quantum Engineering of Optical Nonlinearities

E. Rosencher, A. Fiore, B. Vinter, V. Berger, Ph. Bois, J. Nagle

Second-order optical nonlinearities in materials are of paramount importance for optical wavelength conversion techniques, which are the basis of new high-resolution spectroscopic tools. Semiconductor technology now makes it possible to design and fabricate artificially asymmetric quantum structures in which optical nonlinearities can be calculated and optimized from first principles. Extremely large second-order susceptibilities can be obtained in these asymmetric quantum wells. Moreover, properties such as double resonance enhancement or electric field control will open the way to new devices, such as fully solid-state optical parametric oscillators.

When light is incident on matter, the bound electrons vibrate in the electromagnetic field. While moving under the electromagnetic force, the electrons generate a synchronous polarization field, which interferes with the original field. At low amplitude, this generated field is proportional to the exciting one, and the interference between the driving field and the generated one is the origin of the linear properties of light in matter, such as those described by the optical index of refraction. If the potential that binds the electrons in the material is asymmetric in space, the electron orbits will be distorted relative to the symmetric case, that is, elongated in the direction of the more confining part of the potential. The distorted electron orbits will then generate harmonic

polarization waves (1-3). For instance, a wave at radial frequency  $\omega$  will generate a wave at frequency  $2\omega$ : This is called second-harmonic generation (SHG) and is widely used in the field of nonlinear optics. If we assume a time ( $t$ )-varying electromagnetic field of amplitude  $E$  polarized along the  $z$  axis ( $E e^{-i\omega t} \mathbf{e}_z$ ), the generated SHG polarization  $P_x^{2\omega}(t)$  along the  $x$  axis  $\mathbf{e}_x$  is related to the fundamental electromagnetic field through the relation

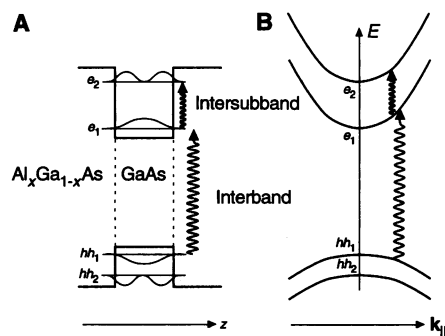
$$P_x^{2\omega}(t) = \frac{\epsilon_0}{2} \chi_{xxx}^{(2)} E_z^2 e^{-2i\omega t} + \text{c.c.} \quad (1)$$

where  $\epsilon_0$  is the vacuum permittivity,  $\chi_{xxx}^{(2)}$  is the second-order optical susceptibility coefficient for SHG in this polarization configuration, and c.c. is the complex conjugate of the first term (4).

The required asymmetry of the electron binding potential is present in naturally

The authors are at Laboratoire Central de Recherches de THOMSON-CSF, Domaine de Corbeville, 91404 Orsay, France.

**Fig. 1. (A)** Energy versus depth  $z$  for a GaAs/ $\text{Al}_x\text{Ga}_{1-x}\text{As}$  heterostructure. Because of the difference in chemical affinities, the GaAs layer, which has a small band gap, behaves as a potential well for electrons and holes, whereas the  $\text{Al}_x\text{Ga}_{1-x}\text{As}$  layer, with a larger band gap, acts as a potential barrier. When the GaAs layer is thin enough, the particle energies corresponding to the motion along the  $z$  growth axis are quantized into levels:  $e_1, e_2, \dots$  for electrons and  $hh_1, hh_2, \dots$  for holes. **(B)** The carrier motion parallel to the interface is free and therefore a kinetic energy must be added to the quantized energy levels  $e_i$  and  $hh_i$ , which are thus the bottom of subbands with quadratic dependence with the parallel wavevector  $\mathbf{k}_\parallel$ . Optical transitions between electron (or hole) subbands are intersubband transitions and, given that the electron (or hole) subbands are parallel, lead to a single-photon energy absorption,  $e_2 \rightarrow e_1$ , for instance. Optical transitions between electron and hole subbands (interband transitions) involve bands of opposite convexity and are therefore distributed in energy.



asymmetric crystal structures such as  $\text{KPO}_3$  and  $\text{LiNbO}_3$  and in chemically engineered organic crystals such as POM (3-methyl-4-nitropyridin-1-oxide) (5). Despite the large number of possible applications, optical frequency conversion (such as frequency doubling) by optical nonlinearities has not resulted in large-scale applications, mainly because the processability of these nonlinear materials is not industrially mature. Here, we review a different way of synthesizing artificially asymmetric structures that is based on semiconducting heterostructures, where the asymmetries are engineered and optimized for any given wavelength or specific application. These structures have novel properties such as giant double-resonance effects and allow the development of new phase-matching techniques. The field can profit from the know-how of the semiconductor industry, potentially leading to large-scale applications of nonlinear optical conversions.

To create an effective potential for electrons, one uses the different band gaps of different semiconductors. The basic building block is therefore the heterojunction of two semiconductors, which is obtained when one semiconductor is grown on top of another so that there is an abrupt interface between the two and perfect conservation of crystallinity. The fabrication of heterojunctions is made possible by modern techniques of semiconductor epitaxy, which allow the growth of alternating layers of different semiconductors with thicknesses that can be controlled down to one atomic layer (6). The most studied semiconductor system is GaAs/AlGaAs; others include InP/InGaAs/InAlAs and Si/Ge. The band gap is an intrinsic property of each semiconductor and is not changed by the interface, but at the interface, there will be a discontinuity between the two conduction bands and a discontinuity between the valence bands. The partition between the conduction- and valence-band discontinuities is determined by the local chemistry on an atomic scale and generally has to be determined experi-

mentally. For an electron in the conduction band of such a heterostructure, the discontinuity results in a step in potential energy. It is therefore possible, with a suitable succession of layers of different semiconductors, to tailor, within limits, any potential profile. The structures of interest for nonlinear optics are quantum wells (QWs), which are formed by growing series of very thin layers of different materials (Fig. 1A). If the width of the potential well formed by the material with the smaller band gap is less than the deBroglie wavelength of the electrons or holes in the material (for example, less than  $\approx 15$  nm for electrons in GaAs), the motion of the carriers can be considered as quantized in the direction normal to the growth axis, whereas in the plane of the quantum wells, their motion is still free (6). Consequently, the wave functions of the electrons and holes are given by a triple product: a periodic part that describes the diffraction of the carriers by the periodic potential of the crystal (which strongly depends on the host crystal), a two-dimensional free wave function that describes the free motion parallel to the QWs, and an envelope wave function that describes the quantized motion of the carriers normal to the QWs (7).

### The Quantum Mechanics of Semiconductor Quantum Wells

Here we use, for the sake of clarity, a simple two-band Kane semiconductor model (7). Consequently, we neglect nonparabolicity and do not consider holes in the valence band with different masses. These subtleties could be introduced at the expense of physical clarity. Having these restrictions in mind, we can write the wave functions of the bound electron and hole states in a QW grown along the  $z$  direction as

$$|e_n, \mathbf{k}_\parallel\rangle = e_n(z)u_c(\mathbf{r})e^{i\mathbf{k}_\parallel\cdot\mathbf{r}_\parallel} \quad (2a)$$

$$|hh_m, \mathbf{k}_\parallel\rangle = hh_m(z)u_v(\mathbf{r})e^{i\mathbf{k}_\parallel\cdot\mathbf{r}_\parallel} \quad (2b)$$

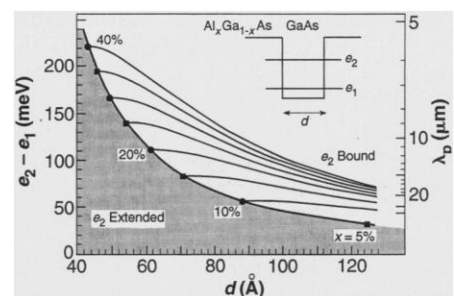


**Fig. 2.** Intersubband optical transition energies (from  $e_2$  to  $e_1$ ) in GaAs/ $\text{Al}_x\text{Ga}_{1-x}\text{As}$  QWs as a function of QW thickness  $d$  and Al concentration  $x$  in the barrier (each curve differs by 5%). The QW parameters (thickness and Al concentration) can be adjusted during growth to meet any wavelength requirement between 5 and 20  $\mu\text{m}$ . The corresponding photon wavelength  $\lambda_p$  is given on the right.

where  $u_c$  and  $u_v$  are the periodic parts of the Bloch functions in the conduction and valence bands, respectively, near the center of the crystal Brillouin zone (at wave vector  $\mathbf{k} = 0$ ),  $\mathbf{k}_\parallel$  is the wave vector in the  $xy$  plane, and the space coordinate  $\mathbf{r} = (r_\parallel, z)$ . The electron and heavy hole envelope wave functions  $e_n(z)$  and  $hh_m(z)$  are the  $n$ th and  $m$ th solutions of the one-dimensional Schrödinger equation in the  $z$ -growth direction:  $H_e e_n(z) = e_n e_n(z)$  and  $H_{hh} hh_m(z) = hh_m hh_m(z)$ , where  $e_n$  and  $hh_m$  are the transverse energy of the  $n$ th conduction subband and  $m$ th valence subband, respectively. The  $z$ -dependent part of the Hamiltonians are  $H_e = p_z^2/2m_e + V_e(z)$  and  $H_{hh} = p_z^2/2m_{hh} + V_h(z)$ , where  $p$  is the particle momentum,  $m_e$  and  $m_{hh}$  are the conduction and heavy hole band effective masses, and  $V_e(z)$  and  $V_h(z)$  represent the profile of the conduction- and valence-band potentials, respectively. The eigenenergies of the Schrödinger equation in the effective-mass Hamiltonian approximation are thus given by

$$E(e_n, \mathbf{k}_\parallel) = e_n + \frac{\hbar^2 \mathbf{k}_\parallel^2}{2m_e} + E_g \quad (3a)$$

$$E(hh_m, \mathbf{k}_\parallel) = -hh_m - \frac{\hbar^2 \mathbf{k}_\parallel^2}{2m_{hh}} \quad (3b)$$

where  $E_g = \hbar\omega_g$  is the band gap of the bulk material and  $\hbar$  is the Planck constant; the second terms in Eqs. 3a and 3b represent the kinetic energies of motion parallel to the interfaces.

In the QWs, the electrons and holes are thus distributed over energy subbands (Fig. 1B): The electron subbands are parallel to each other and have a positive convexity, whereas the hole subbands, which are also parallel to each other (within the two-band model), have a negative convexity. Two different types of optical transitions may thus take place in these QWs, depending on whether the initial and the final states belong to the same band or not.

## Intersubband Optical Transitions in Quantum Wells

We first consider the case where the initial and final states originate from the same band—for instance, the conduction band. Because the ground states are a priori unoccupied, the QWs must be doped so that the electrons given by the donors occupy states in the ground subband. Typical doping densities are  $10^{11}$  to  $10^{12}$   $\text{cm}^{-2}$  per well. Because the subbands are parallel and the optical transitions conserve parallel momentum, the absorption is resonant at a photon energy given by the energy separation between the subbands:  $\hbar\omega_{12} = e_2 - e_1$  (Fig. 1B). In other words, although the electron states originate from a three-dimensional continuum, all of the transitions have the same energy: Consequently, for intersubband transitions, a QW behaves as a purely one-dimensional quantum system. Figure 2 shows the energies of electron intersubband transitions in the GaAs/AlGaAs system as a function of QW thickness and aluminum concentration  $x$ . The higher the Al content in the barrier, the higher are the band discontinuities and the intersubband transition energy. The system parameters can be tailored during growth to tune the transition wavelength to any given value between 5 to 20  $\mu\text{m}$  (including the important wavelength range of 8 to 12  $\mu\text{m}$ , corresponding to the atmospheric transparency window).

The optical dipolar matrix elements that describe the light coupling strength between the initial  $|i\rangle$  and final  $|f\rangle$  states of wave functions  $\varphi_i(\mathbf{r})$  and  $\varphi_f(\mathbf{r})$  are defined as (8)

$$\langle i|q\mathbf{r}|f\rangle = \iiint \varphi_i^*(\mathbf{r})q\mathbf{r}\varphi_f(\mathbf{r})d^3\mathbf{r} \quad (4)$$

where  $q$  is the elementary charge. Because the carriers belong to the same band, the integral in Eq. 4 is dominated by the envelope wave functions (7). This has two consequences.

1) The dipolar terms  $\langle e_1, \mathbf{k}_{\parallel}|x|e_2, \mathbf{k}_{\parallel}\rangle$  and  $\langle e_1, \mathbf{k}_{\parallel}|y|e_2, \mathbf{k}_{\parallel}\rangle$  are zero. The electromagnetic force along the  $x$  or  $y$  axis acting on a free-electron gas is very inefficient (9). The interaction matrix element is then given by (7)

$$\langle e_1, \mathbf{k}_{\parallel}|q\mathbf{E}\cdot\mathbf{r}|e_2, \mathbf{k}_{\parallel}\rangle = E(\cos\alpha)\langle e_1|qz|e_2\rangle \quad (5)$$

where  $\alpha$  is the angle between the electric field of the light beam in the crystal and the growth axis. Note that the integral  $\langle e_1|z|e_2\rangle$  is now performed on the envelope functions and that the periodic parts of the Bloch functions cancel out. The  $\cos\alpha$  coefficient is specific to the electron intersubband transitions and is widely used as a signature of this effect in new heterostructure materials.

2) The dipole extension  $z_{12} = \langle e_1|z|e_2\rangle$  is of the same order of magnitude as the QW

thickness, that is, in the range of a few nanometers. This is extremely large compared to the dipole extension in the host materials (a few angstroms). However, as demonstrated by Khurgin, this intersubband dipole element is comparable to the interband one in a bulk material exhibiting a band gap of the same energy as the intersubband resonance (for example, HgCdTe) (10).

The intersubband absorption was observed for the first time in GaAs/AlGaAs multiquantum wells (MQWs) by West and Eglash (11) and was subsequently used by Levine *et al.* and other groups in a class of infrared photoconductive detectors (12). More recently, cascade lasers have also been demonstrated with the use of stimulated emission between QW subbands (13).

## Interband Optical Transitions in Quantum Wells

The initial states of interband optical transitions are located in the fully occupied valence band, and the final states are in the unoccupied conduction band. Because the energy versus wave vector dispersion curves are of opposite convexity, the absorption is distributed in energy (Fig. 1B). The dipolar matrix elements describing the interband transitions from a heavy hole state  $|hh_n, \mathbf{k}_{\parallel}\rangle$  to an electron state  $|e_m, \mathbf{k}_{\parallel}\rangle$  are now dominated by the periodic Bloch parts and are given by (7)

$$\langle e_m, \mathbf{k}_{\parallel}|q\mathbf{E}\cdot\mathbf{r}|hh_n, \mathbf{k}_{\parallel}\rangle = E\langle e_m|hh_n\rangle\langle u_c|q\mathbf{r}|u_v\rangle \quad (6)$$

Compared to Eq. 5 for intersubband transitions, the main differences are that (i) the  $\cos\alpha$  term is absent, which leads to a dependence on the angle of incidence different from that in the intersubband case,

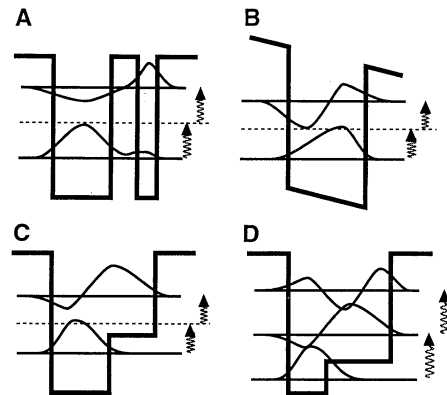


**Fig. 3.** Different configurations of asymmetric quantum wells: (A) asymmetric coupled QWs, (B) electrically biased QWs, and (C) step-asymmetric Al concentration. The arrows symbolize the two-photon process leading to SHG, and the dotted lines represent a virtual state during the transition. (D) The intermediate state is real in the doubly resonant step-QW structure.

and (ii) the dipole extension is dominated by the Bloch term  $\mathbf{r}_{cv} = \langle u_c|\mathbf{r}|u_v\rangle$ , which is of the same order of magnitude as the interatomic distance. Consequently, the interband dipolar moments are much smaller than the intersubband ones in the same material (2).

## Second-Order Optical Nonlinearities in Intraband Transitions in QWs

For intersubband transitions, the dipole matrix elements are in the range of a few nanometers instead of the few picometers obtained in molecular or ionic systems (2). Because second-order optical susceptibilities have a cubic dependence on the dipole matrix elements, strong second-order optical nonlinearities are expected in MQWs, provided that inversion symmetry is broken. This possibility was first addressed by Gurnick and DeTemple, who, in their pioneering work, suggested that one could obtain this asymmetry by growing AlGaAs MQWs with asymmetric composition gradients of Al in the growth direction (14). Many structures have been proposed and analyzed theoretically (Fig. 3) (15–18).

To understand the origins of these huge nonlinearities, we briefly develop the main lines of the quantum calculation of the intersubband SHG coefficient. This calculation is straightforward though cumbersome and leads to the following expression for the second-order susceptibility coefficient (4)

$$\begin{aligned} \chi_{zzz}^{(2)}(2\omega) &= \chi_{2\omega}^{(2)} \\ &= \frac{q^3}{\epsilon_0\hbar^2} \sum_i \sum_k \frac{1}{(2\omega + \omega_{ik}) - i\Gamma} \times \sum_l z_{ik}z_{kl}z_{li} \\ &\quad \left[ \frac{\rho_i - \rho_l}{(\omega + \omega_{il}) - i\Gamma} - \frac{\rho_l - \rho_k}{(\omega + \omega_{lk}) - i\Gamma} \right] \quad (7) \end{aligned}$$

The sums are over all subbands,  $\rho_i$  is the density of carriers occupying the  $i$ th subband, and  $\hbar\omega_{ij}$  are the optical transition energies between subbands  $i$  and  $j$ . For simplicity, the

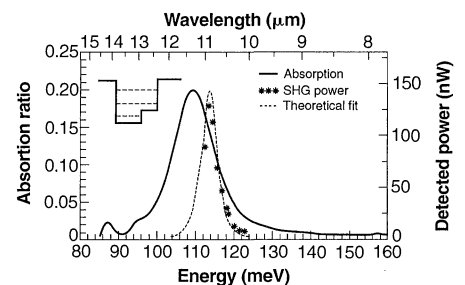


**Fig. 4.** Absorption curve and spectral dependence of SHG in a doubly resonant asymmetrical QW. The SHG coefficient ( $\chi^{(2)} = 750$  nm/V) is 1800 times that of the host material (GaAs). (Inset) Schematic energy band diagram of the structure.

broadening  $\hbar\Gamma$  has been taken to be identical for all of the transitions. As a result of the intersubband selection rules, only the  $zxx$  element is nonzero. We analyze two cases that lead to large nonlinear effects.

1) Simple resonance occurs when the SHG frequency  $2\omega$  is resonant with the single-transition energy ( $\omega_{12} \approx 2\omega$ ) (Fig. 3, A through C). A single term is dominant in Eq. 7 (16)

$$\xi_{2\omega}^{(2)} = \frac{q^3(\rho_1 - \rho_2)}{\epsilon_0 \hbar^2} \frac{z_{12}^2 \delta_{12}}{(\omega - \omega_{12} - i\Gamma)(2\omega - \omega_{12} - i\Gamma)} \quad (8)$$

where  $\delta_{12} = \langle e_1 | z | e_1 \rangle - \langle e_2 | z | e_2 \rangle$  is the spatial separation between the mean electron position in subbands 1 and 2: it is the mean electron displacement during the optical transition. Of course, if the QW is symmetrical, this displacement is zero.

2) Double resonance occurs when the pump frequency  $\omega$  is resonant with the frequency of the transition from the fundamental to first excited state ( $\omega_{12}$ ), and the SHG frequency  $2\omega$  is resonant with the frequency of the transition from the fundamental to second excited state ( $\omega_{13}$ ), requiring  $\omega \approx \omega_{12} \approx \omega_{23}$ . The second-order susceptibility in this case is given by (18)

$$\chi_{2\omega}^{(2)} = \frac{q^3(\rho_1 - \rho_2)}{\epsilon_0 \hbar^2} \frac{z_{12} z_{23} z_{31}}{(\omega - \omega_{12} - i\Gamma)(2\omega - 2\omega_{12} - i\Gamma)} \quad (9)$$

Once again, the product  $z_{12} z_{23} z_{31}$  is identically zero for symmetric QWs. From comparison of the enhancement of the maximum SHG coefficients resulting from the double-resonance effect to those from the singly resonant one at the peak values ( $\omega \approx \omega_{12}$ )

$$\left| \frac{\chi_{2\omega, \max}^{(2)}}{\xi_{2\omega, \max}^{(2)}} \right| = \frac{|z_{12} z_{23} z_{31}| \omega_{12}}{z_{12}^2 \delta_{12} 2\Gamma} \quad (10)$$

it is evident that apart from the geometrical factor  $|z_{12} z_{23} z_{31} / z_{12}^2 \delta_{12}|$ , the main gain in the doubly resonant structure results

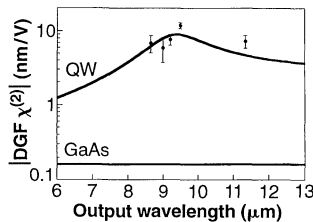


**Fig. 5.** Measured (points) and theoretical (solid curve) coefficients of DFG between  $1.92 \pm 0.25 \mu\text{m}$  and  $2.39 \pm 0.39 \mu\text{m}$  radiations in strained InGaAs/AlGaAs asymmetric coupled QWs (26).

from the long lifetime  $\Gamma^{-1}$  of the electrons in the intermediate level  $e_2$  compared to the resonance period  $\omega_{12}^{-1}$ .

To maximize the second-order susceptibility, one must compromise between the dipolar elements  $z_{12}$  and  $\delta_{12}$  (Eq. 8): An increase of the QW asymmetry will enhance the mean electron displacement  $\delta_{12}$  but it will also decrease the overlap integral in  $z_{12}$ . The optimization leads to a quantum limitation in the second-order susceptibilities that is quite different in nature from earlier models (19), for example, the (nonquantum) "polarizable sphere" model, which yields a  $(\hbar\omega)^{-2}$  dependence of  $\chi_{2\omega}^{(2)}$  (14).

### Mid-Infrared Light Conversion by Intersubband Transitions in QWs

The first experimental evidence of the huge quadratic susceptibility associated with intersubband transitions in QWs was provided by Fejer *et al.* for single resonance (20). They studied the SHG of biased GaAs/AlGaAs quantum wells (Fig. 3B) as a function of applied electric field at intersubband transition energies associated with wavelengths between 9.6 and 10.8  $\mu\text{m}$ ; they obtained measured SHG coefficients as high as 28 nm/V, 73 times larger than those of the bulk GaAs host material. Much larger enhancements were demonstrated by Rosencher *et al.* (18) and Boucaud *et al.* (21) in doubly resonant asymmetric step QWs (Fig. 3D). Figure 4 shows the absorption curve of a doubly resonant structure, which exhibits a Lorentzian lineshape with a total broadening of 10 meV, together with the SHG yield versus pump wavelength curve, which is also clearly resonant. The peak SHG coefficient is as high as 720 nm/V, 1800 times that of GaAs.

Capasso and co-workers thoroughly investigated the large nonlinear optical properties of asymmetric coupled InP/InGaAs/InAlAs quantum wells (Fig. 3A) in the 8- to 12- $\mu\text{m}$  range (22). In a doubly resonant structure, they obtained an SHG coefficient of 75 nm/V, 100 times that of InP. Far-infrared (IR) difference frequency generation was also demonstrated by the same team by mixing two CO<sub>2</sub> lasers in doubly resonant QWs (23).

Most of the above measurements were done in the 8- to 12- $\mu\text{m}$  range. This is because the confining potential of the barriers, which has a chemical origin, is in practice limited to  $\approx 350$  meV in the GaAs/AlGaAs system (6) [corresponding to a maximum SHG photon energy of  $\approx 120$  meV for the double-resonance condition (19)] and to  $\approx 500$  meV in the InP/InGaAs system. To circumvent this difficulty, Chui *et al.* studied highly strained InGaAs/AlAs heterostructures grown on GaAs, for which the confinement potential can be as high as

1.4 eV and the intersubband transition energies have been observed to be as high as 400 meV (24). In this system, Chui *et al.* have demonstrated SHG (25) and difference frequency generation (DFG) of light with wavelengths of  $8.66$  to  $11.34 \mu\text{m}$  by mixing wavelengths of  $1.92 \pm 0.25 \mu\text{m}$  and  $2.39 \pm 0.39 \mu\text{m}$  (26). The experiment was performed with a doubly resonant structure where the  $e_1 \rightarrow e_2$  transition corresponded to the generated  $\omega_3 \approx 10\text{-}\mu\text{m}$  wavelength and the  $e_1 \rightarrow e_3$  transition corresponded to the  $\omega_1, \omega_2 \approx 2\text{-}\mu\text{m}$  pump wavelengths. A peak DFG second-order nonlinear susceptibility  $\chi^{(2)}(\omega_1 - \omega_2 = \omega_3)$  as high as 12 nm/V was measured (Fig. 5). This demonstration of mid-IR DFG is very promising because it opens the way to monolithic diode laser pumps and compact waveguide frequency converters as tunable room-temperature mid-IR sources.

It has been questioned, however, whether one could practically profit from these huge nonlinearities (27). Indeed, the interaction lengths between a nonlinear crystal and a pump laser beam are usually in the millimeter range. Because the absorption coefficients for intersubband transitions are around  $10^4 \text{ cm}^{-1}$ , both the pump ( $\omega$ ) and the doubled ( $2\omega$ ) signals would be strongly absorbed. This problem has been addressed by DeTemple *et al.* (28), Boucaud and Julien (29), and Rosencher (30). Particular to the problem is that the SHG coefficients are so high in these doubly resonant systems that usable SHG yield may be obtained even for interaction lengths smaller than the absorption lengths. Theoretically, conversion efficiencies as large as 20% should be obtainable with an interaction length of a few micrometers but for pumping power near 10 MW/cm<sup>2</sup>.

Fejer *et al.* recently proposed a way to avoid the inherent absorption (31). Singly resonant AQWs can be inserted into the core of a waveguide. The pump power would not be absorbed because of the lack of double resonance. The still important

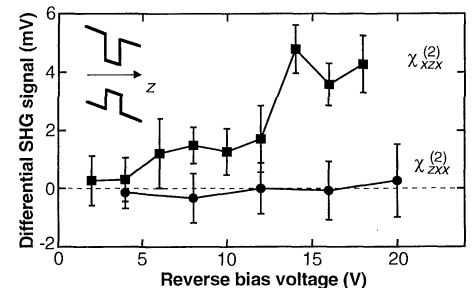


**Fig. 6.** Experimental interband SHG signal from 250 GaAs(5 nm)/Al<sub>0.4</sub>Ga<sub>0.6</sub>As QWs as a function of reverse voltage in the  $\chi_{zxx}^{(2)}$  and the  $\chi_{zxx}^{(2)}$  configurations for a pump wavelength of 1.56  $\mu\text{m}$ . The SHG signal is around 20 pm/V for a 20 kV/cm applied electric field.

SHG power ( $\chi_{2\omega}^{(2)} = 28 \text{ nm/V}$ ) would be extracted before re-absorption by the QWs if it were coupled into radiation modes: this is the Cerenkov configuration of SHG in waveguides (32). If successful, this system will make possible the production of tunable mid-IR radiation (3 to 12  $\mu\text{m}$ ) by difference frequency conversion of near-IR laser light originating from semiconductor lasers.

## Second-Order Optical Nonlinearities in Interband Transitions in QWs

The calculation of second-order susceptibility attributable to interband transitions is far more difficult because (i) the initial and final states have different Bloch function symmetries, (ii) the oscillator strength is not concentrated at discrete energies, because the initial and final subbands are not parallel, and (iii) all inter- and intraband transitions in both the conduction and the valence band are involved. Assuming that the light propagates in the  $y$  direction and using the polarization selection rules, Khurgin (33) showed that, contrary to the intersubband case, the main  $\chi^{(2)}$  tensor element is  $\chi_{xxx}^{(2)}$ , the expression for  $\chi_{xxx}^{(2)}$  is a generalization of Eq. 7. Khurgin (33) and Fiore *et al.* (34) have shown that the intravalence and intraconduction band transitions interfere destructively. Finally, the expression for  $\chi_{xxx}^{(2)}$  has been cast in a very compact and simple form by Fiore *et al.* (34): Each pair of subbands  $c$  and  $v$  in the conduction and valence bands, respectively, contributes to the second-order susceptibility through

$$\chi_{xxx}^{(2)}(2\omega) = \frac{q^3 i}{\pi \hbar \epsilon_0 L (\hbar \omega_c)^2} \langle e_c | h h_v \rangle \langle h h_v | P^z | e_c \rangle x_{cv}^2 \ln \left[ \frac{\hbar \omega - \hbar \omega_{cv} - i \hbar \Gamma}{2 \hbar \omega - \hbar \omega_{cv} - i \hbar \Gamma} \right] \quad (11)$$

where  $P^z$  is the momentum operator in the  $z$  direction acting on the envelope functions only,  $L$  is the width of the well plus that of the barrier, and the different  $x_{cv}$  and  $\hbar \omega_{cv}$  terms are interband optical transition matrix elements and interband energies, respectively. Equation 11 shows that there is a hope of capitalizing on large-envelope optical dipoles because they still contribute to the interband SHG coefficient. For symmetric QWs, the product  $\langle e_c | h h_v \rangle \cdot \langle e_c | P^z | h h_v \rangle$  is zero and the QWs cannot exhibit interband second-order susceptibility. It is instructive to compare the expression of  $\chi^{(2)}$  for intersubband and interband transitions. First, regarding the dipole moments, the intersubband  $\chi^{(2)}$  involves the product of three large dipoles  $z_{12} z_{23} z_{31}$ , whereas only one of the dipoles is large in the interband  $\langle e_c | P^z | h h_v \rangle x_{cv}^2$  product ( $x_{cv}$  is in the angstrom range). Second, the resonance term is logarithmic in

the interband case, which leads to a much weaker resonance than in the intersubband case: this stems from the distributed nature of the energy density of states in the former case. Third, the double resonance condition cannot be met for the interband case because of the large band gap.

We have calculated the  $\chi_{xxx}^{(2)}$  element using Eq. 11 (34). In a 3-nm GaAs/Al<sub>0.4</sub>Ga<sub>0.6</sub>As QW subjected to an applied field of 20 kV/cm, the peak second-order susceptibility is about 20 pm/V at a frequency of 813 meV, corresponding to half of the fundamental  $hh_1 - e_1$  transition. Equation 11 also predicts a linear dependence on bias field.

The measurements of interband second-order susceptibility are more difficult than the intersubband ones because the expected values of  $\chi^{(2)}$  in the QW are comparable to bulk ones. The first measurements of interband SHG in asymmetric QWs were performed by Janz *et al.* (35) and Qu *et al.* (36). The asymmetry was introduced by the growth of compositionally asymmetric structures. The authors measured similar  $\chi_{xxx}^{(2)}$  and  $\chi_{xxz}^{(2)}$  elements, contrary to theoretical expectation (33). It is likely that the interfaces between the GaAs and the AlGaAs layers themselves introduce an asymmetry leading to a SHG signal. To get unambiguous results, we used electric-field-induced asymmetry in QWs so that the signal from the QWs could be extracted from that of the bulk (37) (Fig. 6). From the SHG signal dependence on the applied bias, an approximately linear dependence of  $\chi_{xxx}^{(2)}$  can be deduced, which is in agreement with theory (34). On the other hand,  $\chi_{xxz}^{(2)}$  is zero within experimental errors, as expected from theory (33). The measurement gives a  $\chi_{xxx}^{(2)}$  element around 20 pm/V for a field of 20 kV/cm.

As expected, the latter value is somewhat disappointing compared to the 750,000 pm/V of the intersubband case. However, for applications, even if the absolute value of the  $\chi_{xxx}^{(2)}$  element is rather small, it is important to note that this value is tunable by an applied electric field. This has important consequences.

## Toward Semiconductor Integrated Optical Parametric Oscillators

Semiconductors have large bulk SHG coefficients, for example, about 50 to 100 pm/V in ZnSe and GaAs. However, these large nonlinearities cannot be used in practical devices because of phase-matching problems (2). In fact, because of the optical dispersion of the nonlinear material, the fundamental and SHG beams have different phase velocities and interfere destructively in the crystal at every coherence length, which is given by  $l_c = \lambda_0/4[n(2\omega) - n(\omega)]$ , where  $\lambda_0$  is the wavelength of the pump beam in vacuum and  $n(\omega)$  is the optical index of the material

at frequency  $\omega$ . In metal oxides such as LiNbO<sub>3</sub>, the natural birefringence attributable to the crystal structure is used to eliminate this phase-matching problem. Such a solution is not possible in practical semiconductors because they are not birefringent. Another solution is to reverse the sign of the  $\chi^{(2)}$  element at every coherence length: This is called quasi-phase matching (38, 39). Such a solution has been applied in metal oxides with the use of local metallurgical or crystallographic changes called domain reversals. We have shown above that such a quasi-phase matching could possibly be performed with the use of spatially periodic applied biases (using a metal grid for instance) with  $\chi^{(2)}$  modulation of the order of 20 pm/V. This opens the way to the realization of integrated semiconductor wavelength converters, for instance, and generation of tunable infrared radiation by difference frequency conversion from commercial near-infrared sources. This may be important for a wide range of disciplines, including chemistry and biophysics (40).

The quantum engineering of semiconductor heterostructures has allowed researchers to design artificial asymmetric structures. Extremely large intersubband  $\chi^{(2)}$  elements (more than three orders of magnitude larger than those in usual materials) are obtained but are difficult to use because of their highly resonant nature. Smaller  $\chi^{(2)}$  elements have been obtained for interband transitions. This makes possible new phase-matching techniques for future nonlinear optical devices.

## REFERENCES

1. N. Bloembergen, *Nonlinear Optics* (Benjamin, London, 1977).
2. A. Yariv, *Quantum electronics* (Wiley, New York, 1989).
3. Special issue: "Nonlinear Optics," *Phys. Today* **47** (May 1994).
4. R. W. Boyd, *Nonlinear Optics* (Academic Press, New York, 1992).
5. J. Zyss, *Molecular Nonlinear Optics: Materials, Devices and Physics* (Academic Press, Boston, 1994).
6. C. Weisbuch and B. Vinter, *Quantum Semiconductor Structures: Fundamentals and Applications* (Academic Press, Boston, 1991).
7. G. Bastard, *Wave Mechanics Applied to Semiconductor Heterostructures* (Les Editions de Physique CNRS, Paris, 1988).
8. C. Cohen-Tannoudji, B. Diu, F. Laloë, *Mécanique Quantique* (Hermann, Paris, 1973).
9. J. M. Ziman, *Principles of the Theory of Solids* (Cambridge Univ. Press, Cambridge, 1984).
10. J. Khurgin, *Appl. Phys. Lett.* **62**, 1390 (1993).
11. L. C. West and S. J. Eglash, *ibid.* **46**, 1156 (1985).
12. B. F. Levine, *J. Appl. Phys.* **74**, R1 (1993); E. Rosencher *et al.*, *IEEE J. Quantum Electron.* **30**, 2875 (1994).
13. J. Faist *et al.*, *Science* **264**, 553 (1994).
14. M. K. Gurnick and T. A. DeTemple, *IEEE J. Quantum Electron.* **19**, 791 (1983).
15. J. Khurgin, *Second-Order Intersubband Nonlinear Optical Susceptibilities of Asymmetric Quantum Well Structures*, vol. 10 of *Quantum Wells for Optics and Optoelectronics* (Optical Society of America, Washington DC, 1989), p. 69.
16. D. Ahn and S. L. Chuang, *IEEE J. Quantum Electron.*

- 23, 2196 (1987).
17. P. F. Yuh and K. L. Wang, *J. Appl. Phys.* **65**, 4377 (1989).
  18. E. Rosencher, P. Bois, J. Nagle, S. Delaître, *Electron. Lett.* **25**, 1063 (1989).
  19. E. Rosencher and P. Bois, *Phys. Rev. B* **44**, 11315 (1991).
  20. M. M. Fejer, S. J. B. Yoo, R. L. Byer, A. Harwit, J. S. Harris, *Phys. Rev. Lett.* **62**, 1041 (1989).
  21. P. Boucaud *et al.*, *Appl. Phys. Lett.* **57**, 215 (1990).
  22. C. Sirtori, F. Capasso, D. L. Sivco, S. N. G. Chu, A. Y. Cho, *ibid.* **59**, 2302 (1991); F. Capasso, C. Sirtori, A. Cho, *IEEE J. Quantum Electron.* **30**, 1313 (1994).
  23. C. Sirtori, F. Capasso, J. Faist, L. N. Pfeiffer, K. W. West, *Appl. Phys. Lett.* **65**, 445 (1994).
  24. H. C. Chui, E. L. Martinet, M. M. Fejer, J. S. Harris, *ibid.* **64**, 736 (1994).
  25. H. C. Chui *et al.*, *ibid.*, p. 3365.
  26. H. C. Chui, G. L. Woods, M. M. Fejer, E. L. Martinet, J. S. Harris, *ibid.* **66**, 265 (1995).
  27. Z. Ikonic, V. Milanovic, D. Tjapkin, *IEEE J. Quantum Electron.* **25**, 54 (1989).
  28. T. A. DeTemple, L. A. Bahler, J. Osmundsen, *Phys. Rev.* **24**, 1950 (1981).
  29. P. Boucaud and F. H. Julien, *J. Phys.* **III 1**, 13 (1991).
  30. E. Rosencher, *J. Appl. Phys.* **73**, 1909 (1992).
  31. M. M. Fejer, L. Mei, G. Woods, E. Anvar, T. Pinguet, private communication.
  32. P. K. Tien, R. Ulrich, R. J. Martin, *Appl. Phys. Lett.* **17**, 447 (1970).
  33. J. Khurgin, *Phys. Rev. B* **38**, 4056 (1988).
  34. A. Fiore, E. Rosencher, B. Vinter, D. Weill, V. Berger, *Phys. Rev. B* **51**, 13192 (1995).
  35. S. Janz, F. Chatenoud, R. Normandin, *Opt. Lett.* **19**, 622 (1994).
  36. X. H. Qu, H. Ruda, S. Janz, A. J. SpringThorpe, *Appl. Phys. Lett.* **65**, 3176 (1994).
  37. A. Fiore, E. Rosencher, V. Berger, J. Nagle, *ibid.*, in press.
  38. J. A. Armstrong, N. Bloembergen, J. Ducuing, P. S. Pershan, *Phys. Rev.* **127**, 1918 (1962).
  39. M. M. Fejer, G. A. Magel, D. H. Jundt, R. L. Byer, *IEEE J. Quantum Electron.* **28**, 2631 (1992).
  40. M. M. Fejer, *Phys. Today* **47**, 25 (May 1994).

# Immunology Taught by Viruses

Rolf M. Zinkernagel

The survival of viruses depends on the survival of susceptible hosts. The vertebrate immune system and viruses have therefore coevolved complementary facets. Evidence from various balanced virus-host relationships illustrates that immunological specificity and memory may best be defined biologically and that the mature immune system does not discriminate between "self" and "nonself." Rather, B cells distinguish antigen patterns, whereas T cell responses depend on localization, transport, and kinetics of antigen within lymphatic organs.

Historically, immunology developed from studies of the pathogenesis and prevention of infectious disease (1). The need for purified antigens, which were not available from infectious agents until recently, led to the introduction of model antigens into immunology. Responses to model antigens, proteins, haptens, and synthetic oligopeptides have been instrumental in identifying many of the ground rules underlying the immune responses (2, 3); however, generalization on the basis of some of these results may be inappropriate, because the responses are not important for the survival of the host. Definitions of specificity, memory, and tolerance, the key parameters of the immune response (1), can now be reevaluated in infectious disease models owing to enormous methodological progress in biochemistry, molecular biology, embryology, and animal physiology. These parameters are reviewed here with the aim of arriving at a concept of immunobiology that reflects the coevolutionary balance reached between the immune system and viruses to guarantee survival of both virus and host (4-10). Three basic scenarios are presented: (i) immunity dominates cytopathic virus, (ii) noncytopathic viruses dominate the immune system,

and (iii) the two scenarios are delicately balanced during acute or chronic infections (5, 11-15) (Fig. 1). The nature of the interaction is influenced by viral parameters, such as cytopathogenicity, kinetics, cell and tissue tropism, susceptibility to other resistance mechanisms (for example, interferons), and host reservoirs; and by variables of the immune system, including the specificity, kinetics, and duration of humoral and cell-mediated immunity (1, 4-10), in association with nonspecific effector mechanisms such as complement, hormone-like factors (interleukins), and phagocytes.

Specific humoral immunity is mediated

by antibodies, which are produced and released into the blood by plasma cells, which in turn are derived from B cells (1, 9, 12-16). These antibodies recognize conformational determinants on proteins, carbohydrates or particulate antigens (such as viruses and bacteria) on mucosal membranes, and in the blood. However, with the exception of lesions, they cannot enter solid tissues. Cellular immunity is mediated by T cells, which differentiate in the thymus to express T cell receptors that are specific for small peptides presented by major histocompatibility complex (MHC) molecules (17, 18). Peptides derived from internal proteins—components of the cell itself or of a virus infecting the cell—are, in general, presented by MHC class I molecules; they are recognized by CD8<sup>+</sup> T cells, which may destroy cells by cytotoxicity or release cytokines (or both). Peptides derived from phagocytized proteins—originating in the host or from infectious agent—are digested and presented by MHC class II molecules. These peptides are recognized by cytokine-releasing CD4<sup>+</sup> T helper cells, which usually are nonlytic. Because of this MHC-restricted recognition, T cells monitor only cell-associated alterations. This characteristic, together with their capacity to recirculate and, after activation, to emigrate into peripheral organs, renders T cells well suited for the surveillance of cellular integrity in solid tissues. Specific recognition of antigen by antibodies and T cells usually initiates powerful nonspecific effector mechanisms that control and eliminate infectious agents by complement activation, recruitment of inflammatory cells, phagocytosis, cell destruction, and interference with cellular function (1).

The critical effector mechanisms for recovery from primary infection, resistance against reinfection, or protection of physiologically immunodeficient young offspring are summarized in Table 1. Cytopathic viruses are stopped most efficiently by soluble, diffusing antiviral interleukins (19) that halt virus replication by rendering surrounding

**Table 1.** Critical immunological effector mechanism for recovery from and resistance to infection.

	Resistance against reinfection	
	Lymphoid organs	Peripheral organs
	<i>Cytopathic virus</i>	
T-dependent cytokines and neutralizing antibodies, both amplifying antiviral effects beyond individual effector cells	Neutralizing antibodies	Activated T cells releasing cytokines
	<i>Noncytopathic virus</i>	
Cytolytic T cells individually lyse cells and stop virus replication; released viral antigens induce additional immune responses. Protection causes host cell damage	Increased neutralizing antibodies, cytotoxic T cell precursors	Activated cytolytic T cells

The author is at the Institute of Experimental Immunology, University of Zurich, Schmelzbergstrasse 12, CH-8091 Zurich, Switzerland.